Array Calibration and Digital Predistortion Training Using Embedded Near-Field Feedback Probes and Orthogonal Coding for Enhancing the Performance of Millimeter-Wave Beamforming Arrays

Ahmed Ben Ayed, *Graduate Student Member, IEEE*, Huixin Jin, *Student Member, IEEE*, Bernard Tung, *Graduate Student Member, IEEE*, Patrick Mitran, *Senior Member, IEEE*, and Slim Boumaiza, *Senior Member, IEEE*

***Abstract*— This letter proposes an active array calibration and digital predistortion (DPD) training method that relies on a series of measurement data captured using near-field (NF) probes embedded within the array to enhance the performance of millimeter-wave (mm-wave) radio frequency (RF) beamforming arrays. These measurements are obtained using phase settings that are based on orthogonal coding to enable the characterization of the linear and nonlinear errors in the array's RF chains. The use of embedded NF probes in the proposed method makes it suitable for infield testing. Specifically, the proposed theory is formulated to allow for beamforming-phase-dependent error calibration as well as array linearization without resorting to element-wise measurement or far-field (FF)-based feedback. Furthermore, the proposed theory does not impose a flat coupling requirement between the NF probes and the array antenna elements. Experimental results are conducted on a custom-built 16-element RF beamforming array with four embedded NF probes and operated at 37.5 GHz. The measurements revealed that applying the proposed calibration method reduced the imbalance in the radiation pattern side lobes by up to 2 dB and achieved comparable performance to element-wise FF-based calibration. Furthermore, the proposed DPD training method enabled increasing the effective isotropic radiated power (EIRP) from 32 to 34.2 dBm while maintaining an error vector magnitude (EVM) below 3.5%.**

***Index Terms*— Calibration, digital predistortion (DPD), near field (NF), orthogonal codes, phased arrays, radio frequency (RF) beamforming, Walsh-Hadamard matrix.**

I. Introduction

PHASED arrays are one of the key enabling technologies for millimeter-wave (mm-wave) wireless communication systems, whereby multiple antenna elements are integrated together to achieve a high-effective isotropic radiated power (EIRP). Several mm-wave radio transceiver prototypes, generally following a radio frequency (RF) beamforming architecture with built-in phase and magnitude control, have been reported in the literature [1], [2], [3]. These works highlight the importance of infield array calibration and the need for digital predistortion (DPD) techniques to enhance the overall performance of mm-wave beamforming transmitters.

Different DPD and calibration methods have been proposed in the literature. Using DPD for RF beamforming arrays, the feedback signal(s) needed to train the DPD function are commonly acquired either using couplers at the power amplifier (PA) outputs [2] or at the far-field (FF) using an FF probe [4]. While these works have demonstrated the effectiveness of DPD to linearize an array of PAs, implementing couplers at the PA outputs or the use of an FF probe can be challenging in practice. Recently, Murugesu et al. [1], Liu et al. [5], and Ben Ayed et al. [6] have proposed to use an array of near-field (NF) probes embedded within the array for infield DPD training. While such an approach can alleviate some of the shortcomings of coupler- and FF-based training methods, it does so at the cost of additional design complexity at the array level. Moreover, [1], [5], and [6] require an NF probe design that has flat coupling to its radiating antenna elements.

Most works on DPD schemes assume that the array is calibrated a priori. Calibration methods for RF beamforming arrays can be classified into two categories: 1) element-wise array calibration [7], [8], [9], [10] and 2) active array calibration [3], [11], [12]. Using element-wise calibration, the array's RF chains are calibrated sequentially one antenna at a time with the remaining elements disabled. Such an approach allows compensating for beamforming-phase-dependent errors attributed to the phase shifter as well as any other errors attributed to, among others, process variation and unequal routing. For instance, Haimerl et al. [8] and Cao et al. [9] suggested the use of an element-wise calibration method where the calibration feedback signal is captured using an NF probe mounted on a calibration tower in the vicinity of the array [8], or an array of NF probes embedded in the transmitting array [9]. While these works enable infield calibration, they are inherently slow, as they rely on element-wise calibration. Moreover, they do not account for errors due to current loading and heating effects. To mitigate these challenges, active array calibration has been proposed in the literature where the array's RF chains are calibrated simultaneously.

Manuscript received 27 February 2023; accepted 29 March 2023. This work was supported in part by the Ontario Research Funds-Research Excellence and in part by the Natural Sciences and Engineering Research Council of Canada (NSERC). *(Corresponding author: Ahmed Ben Ayed.)*

The authors are with the Department of Electrical and Computer Engineering, University of Waterloo, Waterloo, ON N2L 3G1, Canada (e-mail: abenayed@uwaterloo.ca).

This article was presented at the IEEE MTT-S International Microwave Symposium (IMS 2023), San Diego, CA, USA, June 11–16, 2023.

Color versions of one or more figures in this letter are available at https://doi.org/10.1109/LMWT.2023.3264877.

Digital Object Identifier 10.1109/LMWT.2023.3264877

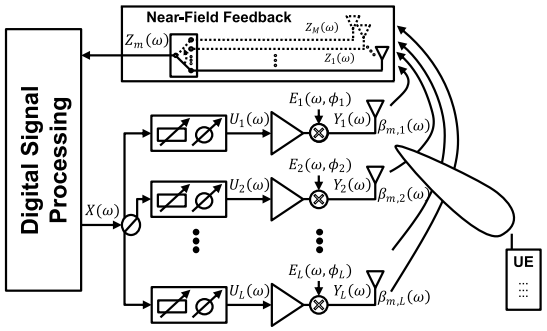

Fig. 1. Block diagram of RF beamforming array with embedded NF probes for array calibration and DPD training.

In [3], [11], and [12], an active array calibration method that uses orthogonal coding and a series of measurements at the FF is proposed. Despite the promising results achieved using this method, the reliance on an FF probe hinders its applicability to infield testing. Moreover, such an approach is not suitable to calibrate for beamforming-phase-dependent errors.

In this work, a novel active array calibration and DPD training method that utilizes NF probes embedded within the array to serve as feedback for infield testing is presented. The proposed method is based on orthogonal codes and can characterize the linear and nonlinear errors in the array's RF chains. The proposed theory is formulated to allow for phase-dependent error calibration as well as array linearization without resorting to element-wise calibration or FF probing. Furthermore, the proposed theory does not impose a flat coupling requirement between the NF probes and the array antenna elements. The performance of the proposed calibration and DPD training method is validated experimentally on a custom-built RF beamforming array with 16 antenna elements and four embedded NF probes.

II. Theoretical Formulation

Fig. 1 shows a block diagram of an RF beamforming array with embedded NF probes. The subscript $\ell \in \{1, \ldots, L\}$ is used to refer to the ℓth RF chain in the array, where L is the total number of antenna elements, while the subscript $m \in \{1, \ldots, M\}$ is used to refer to the mth NF probe, where M is the total number of NF probes. For simplicity, the derivation is conducted directly in the frequency domain. Let ϕ_ℓ be the beamforming phase of the ℓth RF chain, and let $X(\omega)$ be the array input signal, where ω is the angular frequency. Assuming that the PAs are operated in their linear region (backoff), the ℓth PA output is then given by

$$Y_\ell(\omega) = GX(\omega)E_\ell(\omega, \phi_\ell)e^{j\phi_\ell} \tag{1}$$

where G is the designed PA gain and $E_\ell(\omega, \phi_\ell)$ is a beamforming phase (ϕ_ℓ) and frequency (ω)-dependent complex multiplicative error corresponding to the ℓth RF chain in the array. Note, the error, $E_\ell(\omega, \phi_\ell)$, is assumed to be periodic in the phase ϕ_ℓ, such that

$$E_\ell(\omega, \phi_\ell) \approx E_\ell(\omega, \phi_\ell + \pi). \tag{2}$$

This assumption has been validated on a number of commercially available beamforming ICs that employ active or passive phase shifters.

The received signal by the mth NF probe, $Z_m(\omega)$, is then given by

$$Z_m(\omega) = \sum_{\ell=1}^{L} \beta_{m,\ell}(\omega)GX(\omega)E_\ell(\omega, \phi_\ell)e^{j\phi_\ell} \tag{3}$$

where $\beta_{m,\ell}(\omega)$ is the coupling coefficient between the ℓth antenna element and the mth NF probe. Rewriting (3) in matrix form, we have

$$Z_m(\omega) = GX(\omega)\mathbf{\Phi}\mathbf{B}_m(\omega)\mathbf{E}(\omega, \boldsymbol{\phi}) \tag{4}$$

where $\mathbf{\Phi}$ is the L-length row vector $\mathbf{\Phi} = [e^{j\phi_1}, \ldots, e^{j\phi_L}]$, $\mathbf{B}_m(\omega)$ is an $L \times L$ diagonal matrix with ℓth column and ℓth row entry equal to $\beta_{m,\ell}(\omega)$, and $\mathbf{E}(\omega, \boldsymbol{\phi}) = [E_1(\omega, \phi_1), \ldots, E_L(\omega, \phi_L)]^T$ is the error column vector.

Assuming prior knowledge of the NF coupling coefficients $\beta_{m,i}(\omega)$ (obtained, e.g., from electromagnetic simulation of the array or following the procedure described in [9]) and using a series of L/M measurements with custom phase settings applied to each chain in each measurement, the phase-dependent errors $E_\ell(\omega, \phi_\ell)$ for $\ell = 1, \ldots, 1$ can be estimated. Note that, these custom-selected phases need to be chosen, such that the phase-dependent error, $E_\ell(\omega, \phi_\ell)$ for the ℓth chain, remains constant across the different measurements. To that end, the phase settings used during calibration are selected as either ϕ or $\phi + \pi$, since by (2), these have the same error $E(\omega, \phi)$. The choice between these two settings varies between the L/M measurements and is determined by the Walsh-Hadamard matrix, $\mathbf{H}_n$, where

$$\mathbf{H}_n = \begin{bmatrix} \mathbf{H}_{\frac{n}{2}} & \mathbf{H}_{\frac{n}{2}} \\ \mathbf{H}_{\frac{n}{2}} & -\mathbf{H}_{\frac{n}{2}} \end{bmatrix}. \tag{5}$$

$\mathbf{H}_1 = 1$ and n is a power of 2. Specifically, assuming L and $M < L$ are powers of 2, then so is L/M, and let $\mathbf{H}$ be the $L/M \times L$ matrix $\mathbf{H} = [\mathbf{H}_{L/M}\ \mathbf{H}_{L/M}\ \cdots\ \mathbf{H}_{L/M}]$ obtained by concatenating the Walsh-Hadamard matrix $\mathbf{H}_{L/M}$ M times. Then, the phase setting applied to the ℓth RF chain during the ith measurement is determined by the entry in the ith row and ℓth column of $\mathbf{H}$. If the entry is a 1, then the phase setting is $e^{j\phi}$; otherwise, the entry is -1, and the phase setting is $e^{j(\phi+\pi)} = -e^{j\phi}$. Hence, the applied phase to the ℓth antenna elements at the ith measurement is given by the entry in the ith row and ℓth column of $e^{j\phi}\mathbf{H}$. Consequently, if the signals received from the M NF probes are denoted as $\mathbf{Z}_m(\omega) = [Z_{m,1}(\omega), \ldots, Z_{m,L/M}(\omega)]^T$, where $Z_{m,i}(\omega)$ is the NF received signal at the mth NF probe during the ith measurement, then

$$\begin{bmatrix} \mathbf{Z}_1(\omega) \\ \vdots \\ \mathbf{Z}_M(\omega) \end{bmatrix} = GX(\omega)e^{j\phi} \begin{bmatrix} \mathbf{H}\mathbf{B}_1(\omega) \\ \vdots \\ \mathbf{H}\mathbf{B}_M(\omega) \end{bmatrix} \begin{bmatrix} E_1(\omega, \phi) \\ \vdots \\ E_L(\omega, \phi) \end{bmatrix}. \tag{6}$$

Finally, the error terms, $E_\ell(\omega, \phi)$, in (6) can be estimated using least-squares fit. These are then used to calibrate the array or potentially detect faulty antenna elements. With the array now calibrated and operated in its nonlinear region, the ℓth PA output can now be modeled as follows:

$$Y_\ell(\omega) = GV_\ell(\omega)e^{j\phi_\ell} \tag{7}$$

where $V_\ell(\omega) = X(\omega) + N_\ell(\omega)$, and $N_\ell(\omega)$ is the ℓth PA nonlinear additive error. Consequently, the received signal at

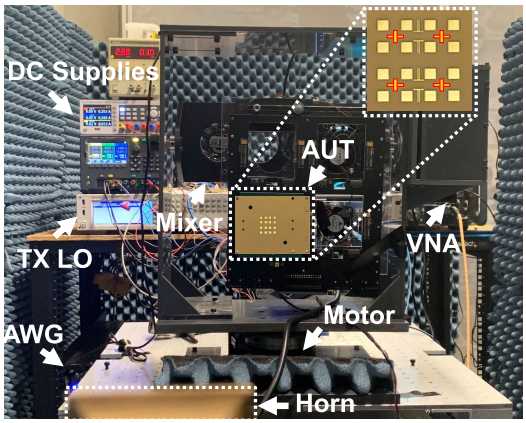

Fig. 2. Over-the-air test setup for experimental validation.

the mth NF probe can be expressed as follows:

$$Z_m(\omega) = G\mathbf{\Phi}\mathbf{B}_m(\omega)\mathbf{V}(\omega) \tag{8}$$

where $\mathbf{V}(\omega) = [V_1(\omega), \ldots, V_L(\omega)]^T$. If now a series of L/M measurements (with phase settings derived from the matrix $\mathbf{H}$) is used with $\phi = 0$, then the received signals may be expressed as follows:

$$\begin{bmatrix} \mathbf{Z}_1(\omega) \\ \vdots \\ \mathbf{Z}_M(\omega) \end{bmatrix} = G \begin{bmatrix} \mathbf{HB}_1(\omega) \\ \vdots \\ \mathbf{HB}_M(\omega) \end{bmatrix} \mathbf{V}(\omega). \tag{9}$$

The PA nonlinear outputs, $\mathbf{V}(\omega)$, in (9) can then be estimated using least-squares fit. These are then summed and used to train the DPD function.

III. Validation Results

In this section, the performance of the proposed calibration and DPD training method is validated experimentally. Fig. 2 shows a picture of the measurement setup. The vector-modulated test signal used in the experiment was generated using a 12-bit, 12-GS/s arbitrary waveform generator (M8190A from Keysight Technologies), with output centered at an intermediate frequency of 2 GHz. An IQ mixer (ADMV-1013) was used to upconvert the IF signal to a center frequency of 37.5 GHz. The signal was then amplified using a driver amplifier followed by a directional coupler and fed to the array under test (AUT). The AUT was mounted on a servo motor. A horn antenna was used to capture the FF signal. The RF outputs of the coupler (i.e., coupled port), the horn antenna, and the NF probes were sampled directly by a vector network analyzer (VNA). A local oscillator source (MXG-N5183B from Keysight Technologies) was used to drive the upconversion board used in the setup. Note that, the array calibration was performed with the AUT input connected to the VNA.

The AUT used in the experiment is a 16-element array with four embedded NF probes. The array was fabricated using a 13-layer printed circuit board with the NF probes located on layer 2 [13] and uses four beamforming integrated circuits (MMW9003KC from NXP) assembled on layer 13. Fig. 2 (inset) shows a picture of the AUT with the location of the NF probes highlighted in red. The modulated measurements were performed using a 400-MHz OFDM signal conforming to 3GPP 5G NR downlink specifications, with subcarriers modulated using 256-QAM, subcarrier spacing of 120 kHz, and

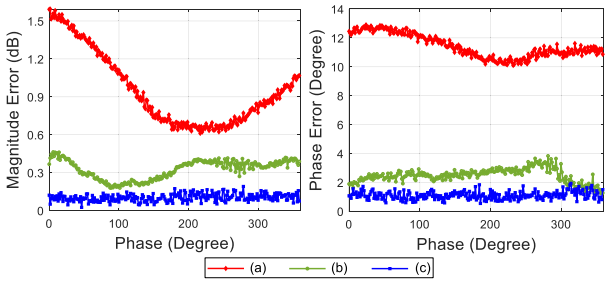

Fig. 3. Measured rms magnitude (left) and phase (right) errors versus phase shifter settings (8 bits)—(a) before calibration, (b) after proposed calibration using NF probes, and (c) after element-wise calibration using an FF probe.

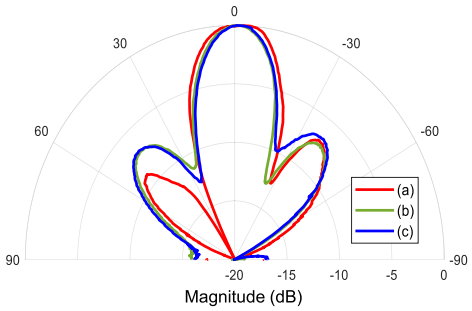

Fig. 4. Measured radiation pattern with the array driven with a 400-MHz OFDM signal and the beam electrically steered from −90° to 90°—(a) before calibration, (b) after proposed calibration using NF probes, and (c) after element-wise calibration using an FF probe.

characterized by a peak-to-average power ratio of 9 dB. For the DPD function, the nonlinearity order, nonlinear memory depth, linear memory depth, and memory step pruning parameters were set to 9, 2, 2, and 1, respectively, resulting in a total of 35 coefficients.

Fig. 3 shows the measured root-mean-square (rms) error in magnitude (left) and phase (right) when the phase states are varied between 0° and 360° in the steps of 1.4°: (a) before calibration, (b) after the proposed calibration using NF probes, and (c) after element-wise calibration using an FF probe. Note that, the rms errors in Fig. 3 are measured element-wise using an FF probe. Using the proposed array calibration method, the rms error in magnitude and phase is reduced by up to 1.3 dB and 10.3°, respectively, compared with before calibration. Using element-wise calibration in Fig. 3(c), the magnitude and phase rms errors are further decreased by at best 0.4 dB and 2.4°, respectively. Fig. 4 shows the measured array radiation pattern at the FF when the array is excited by a 400-MHz modulated signal, and the beam is electrically steered from −90° to 90°: (a) before calibration, (b) after proposed calibration using NF probes, and (c) after element-wise FF calibration. Using the proposed method in Fig. (b), the imbalance in the radiation pattern side lobes was reduced by up to 2 dB. These results are comparable to those obtained using element-wise calibration in Fig. (c).

Fig. 5 shows the adjacent channel power ratio (ACPR) and error vector magnitude (EVM) results at the FF probe versus the EIRP: (a) prior to DPD, (b) after DPD trained at the FF in the main beam direction, and (c) after the proposed NF-based DPD. From Fig. 5, it is evident that the proposed DPD trained using the NF probes in (c) achieved similar results to the DPD trained at the FF (b). For instance, when the EIRP is set to 34 dBm, the ACPR and EVM improved from 27 dB and 8.3% before DPD, to 34.2 dB and 3.1% in (b), and 33.6 dB and 3% in (c), respectively. Note that, using DPD trained with the

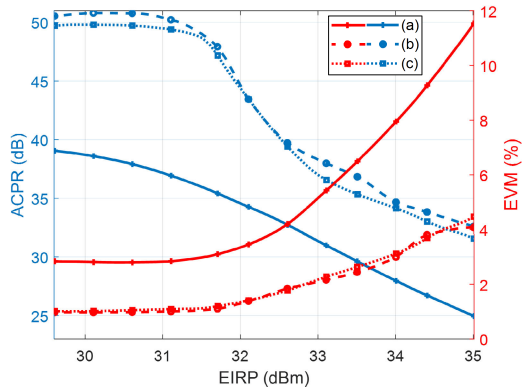

Fig. 5. Measured ACPR and EVM at the FF probe versus EIRP when the array is fed with a 400-MHz OFDM signal—(a) prior to DPD, (b) after DPD trained at the FF in the main beam direction, and (c) after proposed DPD trained using NF probes.

NF probes as feedback, the EIRP increased by 2.3 dB from 32.11 to 33.4 dBm while meeting the 3GPP EVM and ACPR standard of 3.5% and 26 dB requirements.

IV. Conclusion

In this letter, an active array calibration technique and DPD training method that relies on a series of measurement data captured using NF probes embedded within the array to enhance the performance of mm-wave RF beamforming arrays was proposed. The proposed theory was formulated to allow for beamforming-phase-dependent error calibration as well as array linearization without resorting to element-wise measurement or FF-based feedback. Furthermore, the proposed theory does not impose a flat coupling requirement between the NF probes and the array antenna elements. Experimental measurements were conducted on a custom-built 16-element RF beamforming array with four embedded NF probes and operated at 37.5 GHz. These measurements confirmed the ability of the proposed method to characterize and compensate for the linear and nonlinear errors in the array's RF chains.

Acknowledgment

The authors would like to express their gratitude to NXP Semiconductors, Kanata, ON, Canada, for supplying the integrated circuits used in the fabricated array.

References

[1] R. Murugesu, M. Holyoak, H. Chow, and S. Shahramian, "Linearization of mm-wave large-scale phased arrays using near-field coupling feedback for >10 Gb/s wireless communication," in *IEEE MTT-S Int. Microw. Symp. Dig.*, Los Angeles, CA, USA, Aug. 2020, pp. 1271–1274.

[2] X. Liu, W. Chen, L. Chen, F. M. Ghannouchi, and Z. Feng, "Power scalable beam-oriented digital predistortion for compact hybrid massive MIMO transmitters," *IEEE Trans. Circuits Syst. I, Reg. Papers*, vol. 67, no. 12, pp. 4994–5006, Dec. 2020.

[3] Y. Aoki et al., "An intermodulation distortion oriented 256-element phased-array calibration for 5G base station," in *IEEE MTT-S Int. Microw. Symp. Dig.*, Denver, CO, USA, Jun. 2022, pp. 518–521.

[4] E. Ng, Y. Beltagy, G. Scarlato, A. B. Ayed, P. Mitran, and S. Boumaiza, "Digital predistortion of millimeter-wave RF beamforming arrays using low number of steering angle-dependent coefficient sets," *IEEE Trans. Microw. Theory Tech.*, vol. 67, no. 11, pp. 481–484, Jul. 2019.

[5] X. Liu, W. Chen, L. Chen, F. M. Ghannouchi, and Z. Feng, "Linearization for hybrid beamforming array utilizing embedded over-the-air diversity feedbacks," *IEEE Trans. Microw. Theory Techn.*, vol. 67, no. 12, pp. 5235–5248, Dec. 2019.

[6] A. B. Ayed, Y. Cao, P. Mitran, and S. Boumaiza, "Digital predistortion of millimeter-wave arrays using near-field based transmitter observation receivers," *IEEE Trans. Microw. Theory Techn.*, vol. 70, no. 7, pp. 3713–3723, Jul. 2022.

[7] W. T. Patton and L. H. Yorinks, "Near-field alignment of phased-array antennas," *IEEE Trans. Antennas Propag.*, vol. 47, no. 3, pp. 584–591, Mar. 1999.

[8] J. A. Haimerl, B. Hudson, G. P. Fonder, and D. K. Lee, "Overview of the large digital arrays of the space fence radar," in *Proc. IEEE Int. Symp. Phased Array Syst. Technol. (PAST)*, Waltham, MA, USA, Oct. 2016, pp. 1–8.

[9] Y. Cao, A. B. Ayed, J. Xia, and S. Boumaiza, "Uniformly distributed near-field probing array for enhancing the performance of 5G millimeter-wave beamforming transmitters," *IEEE Microw. Wireless Compon. Lett.*, vol. 31, no. 6, pp. 823–826, Jun. 2021.

[10] S.-C. Chae, H.-W. Jo, J.-I. Oh, G. Kim, and J.-W. Yu, "Coupler integrated microstrip patch linear phased array for self-calibration," *IEEE Antennas Wireless Propag. Lett.*, vol. 19, no. 9, pp. 1615–1619, Sep. 2020.

[11] B. Bräutigam, M. Schwerdt, M. Bachmann, and M. Stangl, "Individual T/R module characterisation of the Terrasar-X active phased array antenna by calibration pulse sequences with orthogonal codes," in *Proc. IEEE Int. Geosci. Remote Sens. Symp.*, Barcelona, Spain, Jul. 2007, pp. 5202–5205.

[12] R. Long, J. Ouyang, F. Yang, W. Han, and L. Zhou, "Multi-element phased array calibration method by solving linear equations," *IEEE Trans. Antennas Propag.*, vol. 65, no. 6, pp. 2931–2939, Jun. 2017.

[13] H. Jin, A. B. Ayed, B. Tung, P. Mitran, and S. Boumaiza, "Embedded near-field probing antenna for enhancing the performance of 37–41 GHz linear and dual-polarized phased antenna arrays," in *IEEE MTT-S Int. Microw. Symp. Dig.*, San Diego, CA, USA, Feb. 2023.